THE JOURNAL OF PHYSICAL CHEMISTRY C

ARTICLE

pubs.acs.org/JPCC

CO Oxidation on Positively and Negatively Charged Ag_{13} Nanoparticles

Da Hye Kim, Kihyun Shin, and Hyuck Mo Lee*

Department of Materials Science and Engineering, KAIST, 291 Daehak-ro (373-1 Guseong-dong), Yuseong-gu, Daejeon, Republic of Korea

Supporting Information

ABSTRACT: Utilizing density functional theory calculations and a modified kinetic model, we report the CO oxidation reactivity of negatively and positively charged isolated cuboctahedron (COh) and icosahedron (Ih) Ag_{13} nanoparticles. Charging the nanoparticles modifies the electron distribution in the core and shell atoms as well as the structural stability of the Ag nanoparticles. During the reaction, Ih Ag_{13} nanoparticles can be easily deformed into an amorphous or COh structure, which is more stable than the Ih structure. However, it does not function well as a renewable catalyst. Although a neutral COh Ag_{13} nanoparticle exhibits relatively poor reactivity, the reactivity is enhanced significantly by excess electrons. This study provides fundamental insight into how the electronic and structural interaction between an oxide support and the supported nanoparticle affects the catalytic activity of the general nanocatalyst.

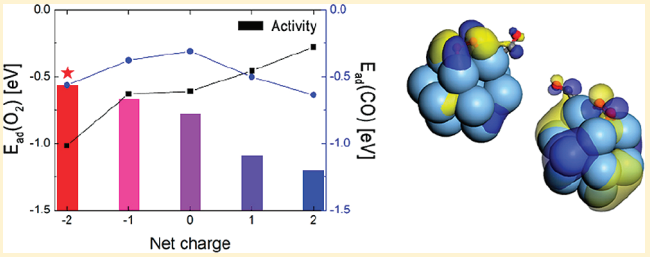

1. INTRODUCTION

Numerous studies on the development and design of catalysts have highlighted how nanoscale materials enhance the performance of catalysts.[1−8] The high surface to volume ratio of nanomaterials causes such materials to have frequent opportunities with the reactants of a targeted chemical reaction and to enhance the catalytic activity. Furthermore, nanoscale materials have a large number of low-coordinated atoms at the surface of these particles, which also leads to a high reactivity.[6−8] The catalytic performance of the nanocatalysts cannot be explained by just one factor. A complicated combination of factors, such as the size, composition, and structure of a nanoparticle, is required to explain catalytic performance. However, the exact nature of their relationship and priority is still debatable.

Unlike metal single crystals, small nanoparticles supported on a metal oxide surface exhibit unique catalytic properties. The electronic properties and the reactivity of these supported catalysts have been previously studied.[9,10] The electronic interaction of the metal nanoparticles with the oxide support induces a change in the charge state of the supported metal nanoparticle. Haruta[3] found that gold nanoparticles could catalyze CO oxidation at or below room temperature. More recent studies on the catalytic property of small nanoparticles have primarily focused on gold nanoparticles. In addition, investigations of how the charge state affects catalytic properties have also targeted gold systems.[11−17] Gold nanoparticles reportedly exhibit different charge states on different supports.[11−17] The type of oxide support and the type of defects present on the oxide surface affect the charge state of supported nanoparticles. Flytzani-Stephanopoulos and co-workers[11] reported that Au and Pt nanoparticles on a ceria support catalyze the water−gas shift reaction. Electrons were transferred from a gold nanoparticle to the ceria, and the positively charged gold nanoparticles exhibited good catalytic properties. The Metiu group[12] also studied the Au/CeO_2 system and positively charged Au nanoparticles. Zhang et al.[13] studied gold nanoparticles supported on stoichiometric and defective ceria supports. They found that gold nanoparticles were negatively charged as a result of the excess electrons from the defects on the ceria surface. Minatoa and co-workers[14] found that negatively charged Au nanoparticles on TiO_2 demonstrated good catalytic activity. The Hammer group[15] and Yoon et al.[5] observed negatively charged gold nanoparticles on a MgO support, whereas Guzman et al.[16] observed positively charged gold nanoparticles on the same type of MgO support. The Dravid group[17] observed negatively charged Au nanoparticles on an Al_2O_3 support.

Clearly, the charge state of supported nanoparticles can be tuned by controlling the oxide support, and the excess charge of a nanoparticle affects the activity of a catalytic reaction on the surface of the nanoparticle. Many of the previously mentioned studies focus on the charge state of nanoparticles under various conditions to observe the changes in the catalytic properties as a function of the charge state. We need to know why the catalytic performance can be improved by changing the charge state and how the supports can be controlled to enhance the catalytic properties. Additionally, recent studies[18,19] have revealed that ligands, which prevent aggregation and allow for synthesis of

Received: August 1, 2011
Revised: November 2, 2011
Published: November 03, 2011

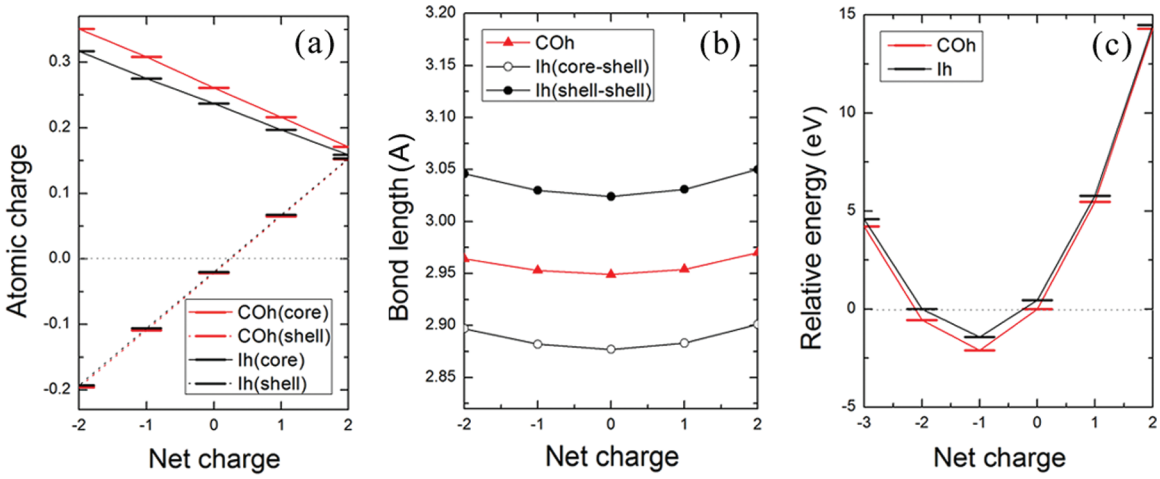

Figure 1. Evolution of (a) the Mulliken atomic charge distributions (the solid line represents the atomic charge of the core atom and the dotted line represents the atomic charge of the shell atom), (b) the bond length between core and shell Ag atoms and the bond length between Ag atoms in the same shell, and (c) the relative energy of COh and Ih Ag_{13} nanoparticles with charge states ranging from (−2) to (+2).

well-controlled nanoparticles, will surround a metal nanoparticle and can affect the electronic configuration of the nanoparticle. This result emphasizes the importance of understanding the relationship between the charge state and the catalytic property of nanocatalysts.

Typically, a catalytic reaction on the surface of a metal nanocatalyst follows the Langmuir−Hinshelwood mechanism[20] involving adsorption of reactants, diffusion of adsorbates on the surface, interaction between adsorbates, and desorption of products. To develop a new catalyst, we need to understand each step of the catalytic reaction. However, it is experimentally difficult to clearly understand the overall process and to determine the rate-determining step. Catalytic reactions occur very quickly. Furthermore, even though the reactants consist of only two gases, these gases can form several intermediates from various reaction pathways. Atomic-scale simulations are useful for probing the details of complicated chemical reactions with fast rates. In addition, considerable information about a nanoscale material including its energetic, electronic, and geometric properties can be obtained. Nørskov and co-workers[21−24] and Campbell et al.[25] employed DFT to explain how the energy levels of intermediates and transition states can control the catalytic reaction rate. Our study is based on DFT calculations and a modified kinetic model.[22,26]

Ag reportedly has a lower catalytic activity than nanosized Au particles.[22] Our previous study[26] also showed that the cuboctahedron (COh) Ag nanoparticle exhibited low CO oxidation reactivity, whereas the good initial reactivity of the icosahedron (Ih) Ag nanoparticle was immediately diminished by a reaction-driven structural change of the Ih structure to an amorphous state. In this study, Ag_{13} nanoparticles with both Ih and COh isomers were designed as a simple model system to investigate the CO oxidation reaction. The structure of the metal nanoparticles can be affected by the support materials.[27,28] However, to clarify the difference in catalytic performance induced by the different initial structures, we excluded other factors in our study. For the positively and negatively charged bare Ag nanoparticle models, the change in the catalytic activity as a function of the excess charge in the supported catalysts was calculated. By controlling the charge state, the CO oxidation reactivity of Ag nanoparticles was found to be similar for Au nanoparticles. In addition, we propose the optimal charge state of the Ag_{13} nanoparticles for CO oxidation.

2. COMPUTATIONAL DETAILS

We performed DFT calculations with the atomic orbital-based Dmol^3 package.[29,30] The spin-polarized Kohn−Sham equation was expanded in a local atomic orbital with a double numeric plus polarization quality basis set. The basis set cutoff was chosen to be 5 Å. The convergence tolerances for the geometry optimization were set to 10^{-5} Ha for the energy, 0.002 Ha/Å for the force, and 0.005 Å for the displacement. The electronic SCF tolerance was 10^{-6} Ha. A Fermi smearing of 0.002 Ha was used in all of the calculations. The DFT semicore pseudopotential proposed by Delley in 2002[31] was employed to treat the core electrons. This potential only replaces the core electrons for heavier elements beginning with Sc possessing a simple potential. The exchange-correlation potential and energy are described in terms of the revised-PBE generalized gradient approximation.[32] The RPBE is specialized for oxidation and numerous other surface chemical reactions involving hydrocarbons. The transition state calculations are based on two synchronous transit methods (i.e., the linear synchronous transit and the quadratic synchronous transit[33]), and the results are refined with a conjugate gradient minimization algorithm. The atomic charge distribution was analyzed by the Mulliken method.[34]

3. RESULTS AND DISCUSSION

3.1. Positively and Negatively Charged Bare Nanoparticles. We examined how the excess charge obtained by interaction between a support and a supported metal nanoparticle affects the electronic and structural properties of Ag_{13} nanoparticles with a COh and Ih structure. Figure 1 shows how the atomic charge distribution, the bond lengths between the Ag atoms in the nanoparticle, and the total energy evolve as the charge state varies. An increase in the negative charge of the COh and Ih nanoparticles causes an increase in the negative charge of the shell atoms and an increase in the positive charge of the core atom. Each excess electron causes the core atom to lose electrons linearly, with an average of 0.045 electrons for the COh particle

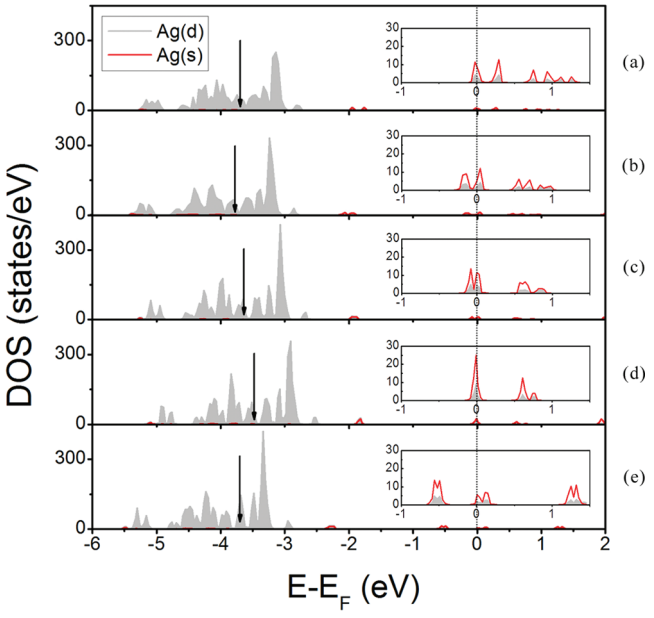

Figure 2. Local density of states (DOS) for charged COh Ag_{13} nanoparticles: (a) (+2), (b) (+1), (c) (0), (d) (−1), (e) (−2). The red solid lines denote the *s*-band of Ag, and the *d*-band of Ag is shown by the shaded areas. The arrows denote the *d*-band center for each charged Ag_{13} nanoparticle. The inserts indicate an enlarged view near the Fermi energy (E_F, the dotted line).

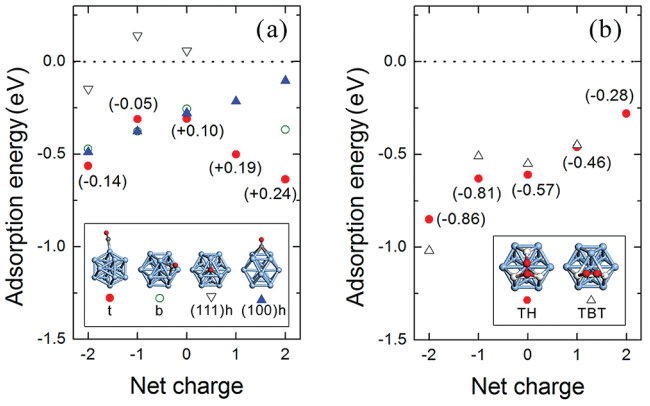

Figure 3. Adsorption energy of (a) CO and (b) O_2 on several adsorption sites of the charged COh Ag_{13} nanoparticles: for CO molecule, on-top (t, filled circles), bridge (b, open circles), (111) hollow ((111)h, open reverse triangles), and (100) hollow ((100)h, filled triangles) sites; for O_2 molecule, top-hollow (TH, filled circles) and top-bridge-top (TBT, open triangles) sites. The values in (a) denote the Mülliken charge of the CO molecule adsorbed on the on-top site and the values in (b) denote the Mülliken charge of the O_2 molecule adsorbed on the TH site for each charge state. The positive value indicates that the electrons are transferred from adsorbates to the metal nanoparticle resulting in a molecule with a positive charge, whereas a negative value indicates the opposite result.

and 0.040 electrons for the Ih particle. Then, the excess electron initially given to the nanoparticle and the electrons obtained from the core atom are redistributed in each shell. The shell atoms have a slightly negative charge even when the nanoparticle is neutral. The coordination number of a shell atom is 5 for the COh nanoparticle and 6 for the Ih nanoparticle. Thus, the shell atoms of the COh nanoparticle require more electrons than those of the Ih nanoparticle,[35] as shown in part a of Figure 1. Therefore, the core atom of the COh nanoparticle is more positively charged than the core atom of the Ih nanoparticle at the same charge state.

When the excess charge on a nanoparticle is positive, the volume of the nanoparticle expands because of the repulsive force between the positively charged core Ag atom and the positively charged shell Ag atoms. When the excess charge of a nanoparticle is negative, the atoms on the surface become more negatively charged, and the repulsive force between the atoms of the shell lengthens the bond between the Ag atoms. The Ih nanoparticle is strained even in a neutral state due to the difference in bond lengths between the shell atoms and between the core and shell atoms. The expansion of the charged Ih nanoparticle increases the bond length differences, and the Ih nanoparticle becomes unstable. In addition, the structure of the charged crystalline nanoparticles, especially the Ih nanoparticle, becomes amorphous as a result of the deformation induced by the adsorbed molecules.

The COh and Ih particles both have a minimum energy at a charge state of (−1), as shown in part c of Figure 1. For all charge states, the COh is more stable. The neutral COh Ag_{13} nanoparticle is 0.449 eV more stable than the neutral Ih nanoparticle. Figure 2 shows the local density of state for the charged COh Ag_{13} nanoparticles. In the charge state of (−1), the interaction between the energy states of the Ag-*d* and the Ag-*s* bands are stronger than the other charge states. The *s*−*d* hybridization strengthens the bond between Ag atoms.[36] The 5*s* band near the Fermi energy (E_F) is not split at a charge state of (−1), but the *d*-band center is higher and the *d*-bandwidth is narrower for a net charge of (−1) compared with other charge states. An increase in the number of excess electrons leads to an increase in the Fermi energy level and in the occupation of the empty *s* and *p* bands of the Ag atoms. E_F is −5.303 eV, −4.241 eV, −3.473 eV, −2.767 eV, and −1.667 eV for the COh Ag_{13} nanoparticles with charge states ranging from (−2) to (+2), respectively.

3.2. Adsorption of CO and O_2 on Charged COh Ag_{13} Nanoparticles. Figure 3 shows the adsorption energy of CO and O_2 molecules as a function of the charge state of COh Ag nanoparticles. We considered several adsorption sites for CO including an on-top site, and a bridge site, as well as (111) and (100) hollow sites. The CO adsorption on the on-top site has the strongest bonds of the various charge states studied. When the excess charge is negative, a bridge site or a (100) hollow site is also preferred. Fielicke et al.[37] reported that a CO molecule generally prefers to adsorb on an on-top site of a transition metal nanoparticle. However, the CO adsorption at higher coordination sites was occasionally observed depending on the transition metal, as well as the size and charge state of the nanoparticle. The interaction between CO and a transition metal nanoparticle has been described as a mixture of the CO 5σ orbital of a highest occupied molecular orbital (HOMO) state with metal d_{z^2} and *s* orbitals and a mixture of metal d_{xz} and d_{yz} orbitals with the CO 2π antibonding state (2π^*).[38] An increase in the charge transferred from the CO 5σ state to the metal weakens the C−O interaction and strengthens the CO adsorption. In addition, an electron backdonation from the metal to the CO 2π^* state strengthens the CO-metal interaction and weakens the C−O bond.[38] Figure 4 shows the density of states for a bare nanoparticle and the adsorption of CO on an on-top site in a COh Ag_{13} nanoparticle with (−2), neutral, and (+2) charge states. For

dx.doi.org/10.1021/jp207338w |J. Phys. Chem. C 2011, 115, 24771–24777

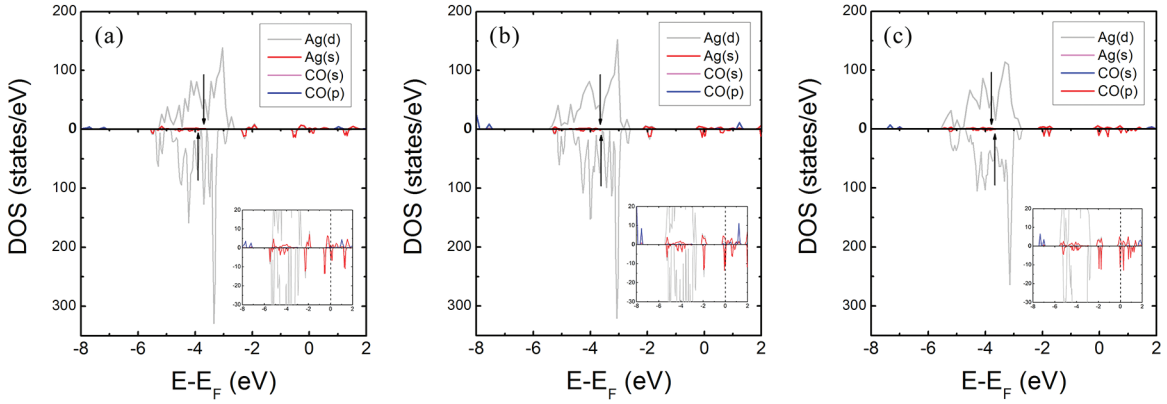

Figure 4. Density of state for a bare COh Ag_{13} nanoparticle and CO adsorbed on an on-top site in the COh Ag_{13} nanoparticle (down and up curves in each panel, respectively) with (a) a negative charge state of (−2), (b) a neutral state, and (c) a positive charge state of (+2). The arrows denote the *d*-band center for each charged Ag_{13} nanoparticle with an enlarged view provided in the inserts.

a (−2) negatively charged nanoparticle, the antibonding state of CO ($2\pi^*$) is located slightly above the E_F, which is shifted down as a result of backdonation, enhancing the stability of the state (part a of Figure 4). The *d*-band center for the metal atoms is shifted up toward the E_F. For a (+2) positively charged nanoparticle, and the *d*-band center and the *s*-band located very close to the E_F for the metal atoms are shifted down after CO adsorption on the metal surface (part c of Figure 4). As a result, we speculate that the CO-metal interaction primarily depends on the π-backdonation for a negative excess charge. Indeed, part a of Figure 3 shows that the Mülliken charge of CO on the on-top site of the negatively charged COh Ag_{13} nanoparticles is a negative value. On the basis of the π-bond between CO and the Ag nanoparticle, we can infer that CO on negatively charged nanoparticles prefers the bridge site or the (100) hollow adsorption site, as well as the on-top site. For neutral and positively charged Ag_{13} COh nanoparticles, the electron donation from CO is dominant. The CO adsorption energy increases when the excess charge is positive or negative.

As shown in part b of Figure 3, we considered two strong adsorption sites for the O_2 molecule, including a top-hollow (TH) site and a top-bridge-top (TBT) site. The O_2 adsorption energy increases as the excess electrons are transferred to the nanoparticle. The TH adsorption site is preferred for most charge states except for the nanoparticle with a (−2) charge. When O_2 is adsorbed on the metal surface, charge transfer occurs from the metal to O_2. All of the Mülliken charges for O_2 in various charge states have negative values. There is an increase in electrons transferred from the nanoparticle to the O_2 molecule when the nanoparticle is more negatively charged (part b of Figure 3; the details are provided in Tables S1 and S2, of the Supporting Information). The negatively charged nanoparticles have more electrons on the surface than the neutral and positively charged nanoparticles. Then, the O_2 on the surface can obtain electrons from just two Ag atoms at the TBT site. Most of electrons transferred to O_2 are from the Ag atoms that are directly involved in the O_2 binding process. The transfer occurs at the TH adsorption site with the top three Ag atoms ($Ag_{3,TH\text{-}top}$, light colored atoms in the left insert of part b of Figure 3) and at the TBT site with the top two Ag atoms ($Ag_{2,TBT\text{-}top}$, light colored atoms in the right insert of part b of Figure 3). The changes in the Mülliken charge of $Ag_{3,TH\text{-}top}$/$Ag_{2,TBT\text{-}top}$ and O_2 are nearly the same in each case (Tables S1 and S2 of the Supporting Information). Furthermore, the charge redistribution induces a structural deformation. The donation of electrons to oxygen causes $Ag_{3,TH\text{-}top}$/$Ag_{2,TBT\text{-}top}$ to be positively charged. Originally, the core atom had a positive charge, and the charge state of the core atom shows very little change as a result of O_2 adsorption. The repulsive force between the positively charged $Ag_{3,TH\text{-}top}$/$Ag_{2,TBT\text{-}top}$ and the core atom causes a local or total expansion of the Ag−Ag bonds. When O_2 is adsorbed on a TBT site of a (+2)-charged COh Ag_{13} nanoparticle, the nanoparticle eventually deforms into an amorphous structure (Tables S1 and S2 of the Supporting Information).

3.3. Adsorption of CO and O_2 Molecules on Charged Ih-Structured Ag_{13} Nanoparticles. The Ih structure is subject to strain caused by a difference in bond lengths between shell atoms and between core and shell atoms. Further stress is added by the adsorption of molecules because the charge transfer between the metal and the adsorbed molecules induces other changes in the structure of the nanoparticle. For CO adsorption on an on-top site, the longitudinal bond is lengthened in a single direction, and the Ag−Ag bonds are broken locally (Figure S1 and Table S3 of the Supporting Information). The Ag atom directly binds to CO, and the opposite Ag atom (atoms A and B in part c of Figure S1 of the Supporting Information) loses electrons after CO adsorption, yet the charge state of the other Ag atoms is only slightly changed. When the nanoparticle is positively charged, the A and B atoms are more positively charged. The repulsive force between the positively charged core and the two shell atoms with a positive charge lengthens the longitudinal bond. For O_2 adsorption on a TBT site, all of the Ih nanoparticles, regardless of their charge, are deformed into an amorphous structure. For O_2 adsorption on TH site of a (−2) negatively charged Ih Ag_{13} nanoparticle, the nanoparticle is also deformed into an amorphous structure (part a of Figure S2 of the Supporting Information). In addition, for O_2 adsorption on a TH site of a (−1) negatively charged Ih Ag_{13} nanoparticle, the nanoparticle is converted into a COh structure (Table 1 and part b of Figure S2 of the Supporting Information). The COh structure is approximately 0.7 eV more stable than the Ih structure with a (−1) charge. We have also calculated the energy barrier for the structural change from an Ih structure to a COh structure. The energy barrier is very low, 0.2 eV. The geometrical change is related to the coordination and the electron density.[35] An anionic nanoparticle has a tendency to have a low coordination because

Table 1. Adsorption Energy of O_2 and CO ($E_{ad}(O_2)$ and $E_{ad}(CO)^*$), the Energy Barrier (E_{barr}) and SA for CO Oxidation on the Charged COh and Ih Ag_{13} Nanoparticles in the Pathway That Exhibits the Highest CO Oxidation Reactivity at Each Charge State; E_{ad} $(CO)^*$ is Based on the Energy Difference between the Coadsorption Energy and E_{ad} (O_2)

	net charge	(−2)	(−1)	(0)	(+1)	(+2)
COh Ag_{13}	pathway	TH-T1	TBT-T1	TBT-T1	TBT-T1	TH-T1
	$E_{ad}(O_2)$ (eV)	−0.85	−0.51	−0.55	−0.45	−0.28
	$E_{ad}(CO)^*$ (eV)	−0.34	−0.29	−0.33	−0.39	−0.33
	E_{barr} (eV)	0.13	0.19	0.33	0.57	0.44
	SA	−0.56	−0.67	−0.78	−1.09	−1.20
	pathway	TH	TH	TH-T1,T2	TH-T1	TH-T1
Ih Ag_{13}	$E_{ad}(O_2)$ (eV)	[a]	[b]	−0.77	−0.63	−0.46
	$E_{ad}(CO)^*$ (eV)			[a]	−0.17	−0.44
	E_{barr} (eV)				0.29	0.52
	SA				−0.89	−0.99

[a] Structural change to amorphous. [b] Structural change to COh.

of the sufficient electron density. Conversely, a cationic nanoparticle has a tendency to exhibit a high coordination. The surface atom of the COh structure has a lower coordination than in the Ih structure. We can speculate that the Ih structure is easily deformed to the COh structure with the addition of electrons. The change from an Ih structure to an amorphous or COh structure is not reversible reversed even if the adsorbed molecules desorb. In our previous study,[26] we observed that the amorphous Ag_{13} nanoparticle has a low reactivity for CO oxidation. The reactivity of CO oxidation on neutral or negatively charged Ih Ag nanoparticles is only good for the first reaction, which is due to a lowering of the system energy caused by the geometrical conversion to an amorphous structure, resulting in a nonreusable catalyst. Therefore, we primarily focused on the details of the COh Ag_{13} nanoparticle in this article.

3.4. CO Oxidation on Charged Nanoparticles. On the basis of the association mechanism[22] that follows the Langmuir−Hinshelwood mechanism, CO oxidation by O_2 molecules can be described as follows:

$$O_2 + * \leftrightarrow O_2* \quad \text{(R1)}$$

$$CO + * \leftrightarrow CO* \quad \text{(R2)}$$

$$CO* + O_2* \leftrightarrow O\text{-}O\text{-}CO* + * \quad \text{(R3)}$$

$$O\text{-}O\text{-}CO* \leftrightarrow CO_2 + O* \quad \text{(R4)}$$

$$CO* + O* \leftrightarrow CO_2 + 2* \quad \text{(R5)}$$

where CO*, O_2*, O−O−CO*, and O* are adsorbed species at the surface and the * represents a free surface site. That is, the coadsorbed CO and O_2 molecules form an intermediate O−O−CO complex[39−41] and then produce CO_2 and an O adatom. Another adsorbed CO molecule subsequently reacts with the O adatom to form one more CO_2 molecule and complete the cycle. To quantify and compare the overall activity of the charged Ag nanoparticles for CO oxidation, we performed

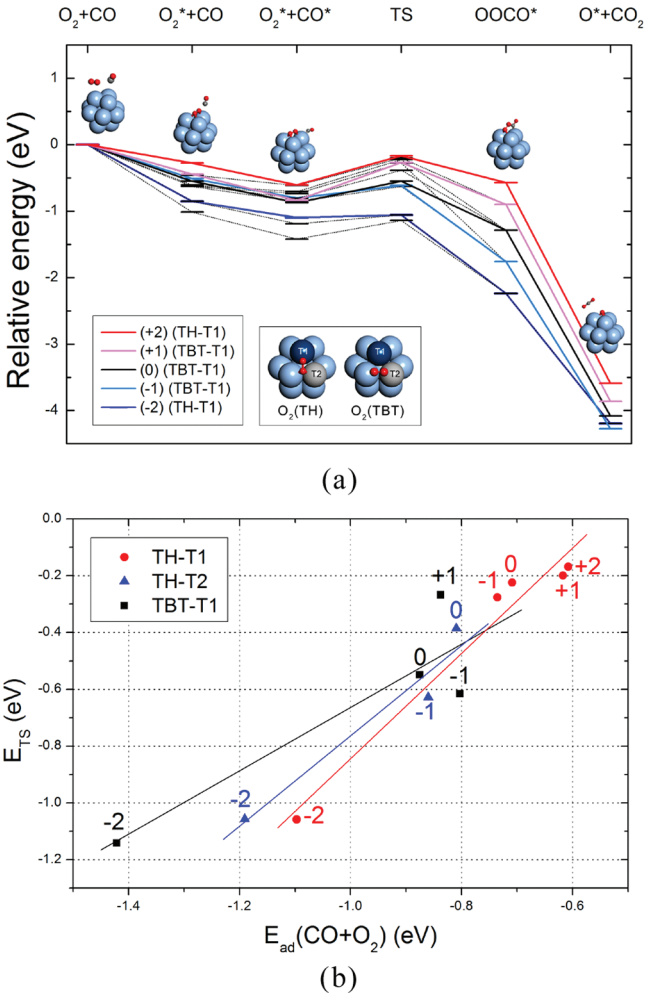

Figure 5. (a) Reaction pathways for CO oxidation on the charged COh Ag_{13} nanoparticles and (b) BEP diagram of the transition state energy (E_{TS}) versus the O_2 and CO coadsorption state energy ($E_{ad}(CO + O_2)$). In (a), the insert denotes the coadsorption sites for O_2 (TH or TBT sites) and CO (T1 or T2 sites) and the inserts along the energy pathway show the reaction pathway for CO oxidation at a TH-T1 site. The solid lines indicate the energy pathway that shows the highest reactivity at each charge state.

a modified microkinetic analysis[26] based on the Sabatier kinetic model.[22,42]

To obtain the Sabatier activity (SA), we need to know the adsorption energy of the reactants (CO and O_2 molecules) and the energy barrier of the rate-determining step (R3), which yields the intermediate O−O−CO complex. In our modified kinetic model, the Sabatier rate of the entire CO oxidation reaction is equal to the maximum rate of R3. As mentioned in sections 3.2 and 3.3, we elucidated the adsorption properties of O_2 and CO individually on charged bare nanoparticles. However, we needed to consider the coadsorption properties of the O_2 and CO molecules. The proportion of O_2 is higher than CO under low-temperature CO oxidation conditions.[22] Assuming that an O_2 molecule is first adsorbed on the bare nanoparticles, the CO molecules must be adsorbed near the preadsorbed O_2 to react with the O_2 molecule in the oxidation reaction. In addition, the CO adsorption energy is derived from the energy difference between the coadsorption energy and the O_2 adsorption energy. Considerable configurations for the coadsorption of O_2 and CO

are shown in the insert of part a of Figure 5. The TBT-T2 pathway was excluded because the nanoparticle was converted to an amorphous form by the coadsorption process. The DFT calculations for the coadsorption energy and the transition state energy were conducted for all of the other pathways, including the TH-T1, TH-T2, and TBT-T1 pathways at each charge state ranging from (−2) to (+2).

Table 1 summarizes the SA as well as the O_2 adsorption energies and the modified adsorption energies of CO with the corresponding energy barrier. All of the SA values were obtained under low-temperature CO oxidation conditions[22] (273 K, p(CO) = 0.01 bar, and p(O_2) = 0.21 bar). As the absolute value of SA decreases, the reactivity improves. The SA of the neutral COh Ag_{13} nanoparticle in the TH-T1, TH-T2, and TBT-T1 pathways is −1.17, −1.00, and −0.78, respectively. The Nørskov group[22] reported that the SA for a CO oxidation reaction of a two-layered, 12-atom Ag nanoparticle is approximately −1.0. Our results are in good agreement with this value. Although the neutral COh Ag_{13} nanoparticle exhibits poor reactivity, a negative (−2) charge state significantly enhances the reactivity, resulting in an SA value of −0.56. Oxygen was adsorbed more strongly on a TBT site than on a TH site for a (−2) charge state (part b of Figure 3). Nevertheless, the overall activity of the reaction that occurs with O_2 on the TH site is higher because of the lower energy barrier for CO oxidation. Because Ih Ag_{13} nanoparticles can be easily deformed by adsorbates, only the SA for positively charged nanoparticles can be determined. Although the structures of positively charged Ih Ag_{13} nanoparticles are not changed during CO oxidation, the nanoparticles show a lower CO oxidation reactivity of −0.89 and −0.99 compared with the COh Ag_{13} nanoparticle in a (−2) charge state. As shown in part b of Figure 5, the results are consistent with the Brφnsted−Evans−Polanyi (BEP) relationship.[43,44]

4. CONCLUSIONS

To understand how excess charge affects atomic-scale catalytic reactivity, we performed DFT calculations for the CO oxidation on COh and Ih Ag_{13} nanoparticles with charge states ranging from (−2) to (+2). An increase of excess electrons causes the shell atoms in both the COh and Ih Ag_{13} nanoparticles to be more negatively charged but causes the core atom in both the COh and Ih to be more positively charged. Because of the redistribution of the charge, the bond lengths between the core and shell atoms or the shell and shell atoms expand when the particle gains or loses excess charge. The COh and Ih Ag_{13} nanoparticles are energetically stable in the (−1) charge state. The CO adsorption energy on a charged nanoparticle is higher than that on a neutral nanoparticle. The CO adsorption property depends more on backdonation rather than on electron donation in the negative charge state and depends more on electron donation in the positive charge state. An O_2 molecule is molecularly adsorbed on the Ag_{13} nanoparticle while taking electrons from the combined metal atoms. The O_2 adsorption energy increases when the nanoparticle is more negatively charged. The energy barrier reaches its lowest value for a (−2) negative charge state. We quantized the catalytic performance by using a modified microkinetic model based on a Sabatier model. As a result, even though the neutral COh Ag_{13} nanoparticle has a poor reactivity for CO oxidation, a catalytic activity of the nanoparticle with a (−2) negative charge is as good as an Au nanoparticle. The fluxional behavior of the Ih Ag_{13} nanoparticle due to excess charge and the adsorption of CO and O_2 resulted in a decrease in the durability and structural stability of the nanocatalyst. The results confirm that we can use excess charge to control the catalytic reactivity of a nanocatalyst. Therefore, our results have important implications for catalysts supported on an oxide support or surrounded by ligands. Further investigations of how oxide supports or capping agents donate excess electrons to Ag nanoparticles could lead to the design of a new catalytic system.

■ ASSOCIATED CONTENT

Supporting Information. Details of O_2 adsorption on the COh Ag_{13} nanoparticle, and additional supporting data and figures for O_2 and CO adsorption on the Ih Ag_{13} nanoparticle. Information about the modified kinetic model is also included. This material is available free of charge via the Internet at http://pubs.acs.org.

■ AUTHOR INFORMATION

Corresponding Author

*Phone: +82-42-350-3334; Fax: +82-42-350-3310; E-mail: hmlee@kaist.ac.kr.

■ ACKNOWLEDGMENT

This research was supported by Future-based Technology Development Program (Nano Fields) through the National Research Foundation of Korea (NRF) funded by the Ministry of Education, Science and Technology (2011-0019163).

■ REFERENCES

(1) Ertl, G. *Angew. Chem., Int. Ed.* **2008**, *47*, 3524–3535.
(2) Lu, Y.-C.; Xu, Z.; Gasteiger, H. A.; Chen, S.; Hamad-Schifferli, K.; Shao-Horn, Y. *J. Am. Chem. Soc.* **2010**, *132*, 12170–12171.
(3) Haruta, M.; Yamada, N.; Kobayashi, T.; Iijima, S. *J. Catal.* **1989**, *115*, 301.
(4) Valden, M.; Lai, X.; Goodman, D. W. *Science* **1998**, *281*, 1647–1650.
(5) Yoon, B.; Häkkinen, H.; Landman, U.; Wörz, A. S.; Antonietti, J.-M.; Abbet, S.; Judai, k.; Heiz, U. *Science* **2005**, *307*, 403–407.
(6) Arenz, M.; Mayrhofer, K. J. J.; Stamenkovic, V.; Blizanac, B. B.; Tomoyuki, T.; Ross, P. N.; Markovic, N. M. *J. Am. Chem. Soc.* **2005**, *127*, 6819–6829.
(7) Jiang, T.; Mowbray, D. J.; Dobrin, S.; Falsig, H.; Hvolbæk, B.; Bligaard, T.; Nørskov, J. K. *J. Chem. Phys. C* **2009**, *113*, 10548–10553.
(8) Janssens, T. V. W.; Carlsson, A.; Puig-Molina, A.; Clausen, B. S. *J. Catal.* **2006**, *240*, 108–113.
(9) Henry, C. R. *Surf. Sci. Rep.* **1998**, *31*, 231–325.
(10) Ishida, T.; Kinoshita, N.; Okatsu, H.; Akita, T.; Takei, T.; Haruta, M. *Angew. Chem., Int. Ed.* **2008**, *47*, 1–6.
(11) Fu, Q.; Saltsburg, H.; Flytzani-Stephanopoulos, M. *Science* **2003**, *301*, 935–938.
(12) Shapovalova, V.; Metiu, H. *J. Catal.* **2007**, *245*, 205.
(13) Zhang, C.; Michaelides, A.; King, D. A.; Jenkins, S. J. *J. Chem. Phys.* **2008**, *129*, 197408.
(14) Minatoa, T.; Susaki, T.; Shiraki, S.; Kato, H. S.; Kawai, M.; Aikaak, K.-I. *Surf. Sci.* **2004**, *566−568*, 1012–1017.
(15) Molina, L. M.; Hammer, B. *Phys. Rev. B* **2004**, *69*, 155424.
(16) Guzman, J.; Gates, B. C. *J. Am. Chem. Soc.* **2004**, *126*, 2672–2673.
(17) Fu, L.; Wu, n. Q.; Yang, J. H.; Qu, F.; Johnson, D. L.; Kung, M. C.; Kung, H. H.; Dravid, V. P. *J. Phys. Chem. B* **2005**, *109*, 3704.
(18) Rodriguez, A.; Amiens, C.; Chaudret, B.; Casanove, M. J.; Lecante, P.; Bradley, J. S. *Chem. Mater.* **1996**, *8*, 1978–1986.

(19) Shafai, G.; Hong, S. Y.; Bertino, M.; Rahman, T. S. *J. Phys. Chem. C* **2009**, *113*, 12072–12078.
(20) Liu, Z. P.; Hu, P.; Alavi, A. *J. Am. Chem. Soc.* **2002**, *124*, 14770.
(21) Greeley, J.; Nørskov, J. K. *J. Phys. Chem. C* **2009**, *113*, 4932–4939.
(22) Falsig, H.; Hvolbæk, B.; Kristensen, I. S.; Jiang, T.; Bligaard, T.; Christensen, C. H.; Nørskov, J. K. *Angew. Chem., Int. Ed.* **2008**, *47*, 4835–4839.
(23) Nørskov, J. K.; Bligaard, T.; Rossmeisl, J.; Christensen, C. H. *Nat. Chem.* **2009**, *1*, 37–46.
(24) Nørskov, J. K.; Bligaard, T.; Kleis, J. *Science* **2009**, *324*, 1655–1656.
(25) Stegelmann, C.; Andreasen, A.; Campbell, C. T. *J. Am. Chem. Soc.* **2009**, *131*, 8077–8082.
(26) Kim, H, Y.; Kim, D. H.; Ryu, J. H.; Lee, H. M. *J. Phys. Chem. C* **2009**, *113*, 15559–15564.
(27) Ferrando, R.; Barcaro, G.; Fortunelli, A. *Phys. Rev. Lett.* **2009**, *102*, 216102.
(28) Ferrando, R.; Rossi, G.; Levi, A. C.; Kuntová, Z.; Nita, F.; Jelea, A.; Mottet, C.; Barcaro, G.; Fortunelli, A.; Goniakowski, J. *J. Chem. Phys.* **2009**, *130*, 174702.
(29) Delley, B. *J. Phys. Chem. C* **1996**, *100*, 6107–6110.
(30) Delley, B. *J. Chem. Phys.* **2000**, *113*, 7756.
(31) Delley, B. *Phys. Rev. B* **2002**, *66*, 155125.
(32) Hammer, B.; Hansen, L. B.; Nørskov, J. K. *Phys.Rev. B* **1999**, *59*, 7413.
(33) Halgren, T. A.; Lipscomb, W. N. *Chem. Phys. Lett.* **1977**, *49*, 225.
(34) Mulliken, R. S. *J. Chem. Phys.* **1955**, *23*, 1833–1846.
(35) Gruene, P.; Rayner, D. M.; Redlich, B.; Van der Meer, A. F. G.; Lyon, J. T.; Meijer, G.; Fielicke, A. *Science* **2008**, *321*, 674.
(36) Hâkkinen, H.; Moseler, M.; Landman, U. *Phys. Rev. Lett.* **2002**, *89*, 033401.
(37) Fielicke, A.; Gruene, P.; Meijer, G.; Rayner, D. M. *Surf. Sci.* **2009**, *603*, 1427–1433.
(38) Hammer, B.; Nørskov, J. K. *Adv. Catal.* **2000**, *45*, 71–129.
(39) Wang, C. M.; Fan, K.-N.; Liu, Z.-P. *J. Am. Chem. Soc.* **2007**, *129*, 2642.
(40) Molina, L. M.; Hammer, B. *Phys. Rev. Lett.* **2003**, *90*, 206102.
(41) Molina, L. M.; Rasmussen, M. D.; Hammer, B. *J. Chem. Phys.* **2004**, *120*, 7673.
(42) Nilson, A.; Pettersson, L. G. M.; Nørskov, J. K. *Chemical Bonding at Surfaces and Interfaces*; Elsevier: Amsterdam, 2008; pp 297−312.
(43) Loffreda, D.; Delbecq, F.; Vign, F.; Sautet, P. *Angew. Chem., Int. Ed.* **2009**, *48*, 8978–8980.
(44) Nørskov, J. K.; Bligaard, T.; Logadottir, A.; Bahn, S.; Hansen, L. B.; Bollinger, M.; Bengaard, H.; Hammer, B.; Sljivancanin, Z.; Mavrikakis, M.; Xu, Y.; Dahl, S.; Jacobsen, C. J. H. *J. Catal.* **2002**, *209*, 275–278.